

---

# Learning to Infer 3D Object Models from Images

---

Chang Chen\*, Fei Deng\*, and Sungjin Ahn  
 Department of Computer Science  
 Rutgers University  
 {chang.chen, fei.deng, sungjin.ahn}@rutgers.edu

## Abstract

A crucial ability of human intelligence is to build up models of individual 3D objects from partial scene observations. Recent works have enabled unsupervised 3D representation learning at scene-level, yet learning to decompose the 3D scene into 3D objects and build their individual models from multi-object scene images remains elusive. In this paper, we propose a probabilistic generative model for learning to build modular and compositional 3D object models from observations of a multi-object scene. The proposed model can (i) infer the 3D object representations by learning to search and group object areas and also (ii) render from an arbitrary viewpoint not only individual objects but also the full scene by compositing the objects. The entire learning process is unsupervised and end-to-end. We also demonstrate that the learned representation permits object-wise manipulation and novel scene generation, and generalizes to various settings.

## 1 Introduction

At the core of human learning is the ability to build up mental models of the world along with the growing experience of our life. A particularly crucial aspect here is to build 3D models of entities like objects and agents—foundational units of the world—even if we can see these only via partial observations. A scene is usually composed of multiple entities with occlusions. But, it is not a problem for us to understand the compositional modular structure of such scenes in terms of individual objects and their relationships. This ability of structurally understanding a scene is believed to be crucial in enabling various advanced cognitive functions in human-like AI systems [32] such as reasoning [3], causal inference [42, 38], imagining the future [27, 24, 41], and out-of-distribution generalization [1, 38].

A particularly relevant work in learning 3D scene representation is the Generative Query Network (GQN) [13]. It learns both the representation and rendering of a 3D scene from partial observations. However, GQN can only provide a scene-level representation without an explicit representation of the object-centric structure of the scene. Other related advances are in object-centric representation learning via unsupervised generative latent variable modeling [12, 17, 50, 29, 9, 8, 23, 34, 30]. Although these models can learn unsupervised decomposition of a scene into object-wise modular representations, only fully-observable 2D scenes can be modeled, leaving the 3D structure of objects and partial observability unaddressed.

In this paper, we tackle the problem of learning to build modular and compositional 3D object models from scene images. Our proposed model, ROOTS (Representation and Rendering of Object-Oriented Three-D Scenes), is able to decompose partial observations into objects, group them object-wise, and build a modular compositional 3D representation of individual objects and their global scene layout in the scene. Such representation also enables compositional rendering—the entire scene can be rendered from arbitrary viewpoints by first rendering individual objects and then compositing them according to the scene layout. In particular, this modeling allows us to reuse the GQN model as

---

\* Equal Contribution

a module for object modeling, making the model simpler. The entire process is unsupervised and end-to-end trainable. We demonstrate the above capabilities of our model on simulated 3D scenes with multiple objects. We evaluate our model in terms of the generation quality, structure accuracy, generalization ability, and downstream task performance. We also showcase that by manipulating the scene layout, we can generate scenes with many more objects than typical of the training regime.

## 2 Preliminary: Generative Query Networks

The Generative Query Network (GQN) is a latent variable model for learning to represent and render 3D scenes. Given a set of context images and viewpoints, GQN learns a *3D representation* that allows generating a target image viewed from an arbitrary viewpoint. Due to this property, it is also called viewpoint-invariant.

Consider an agent navigating a scene and collecting  $K$  pairs of images  $\mathbf{x}_c$  and corresponding viewpoints  $\mathbf{v}_c$  for  $c = 1, \dots, K$ . We refer to this collection as *context*  $\mathcal{C} = \{(\mathbf{x}_c, \mathbf{v}_c)\}_{c=1}^K$ . GQN learns a scene-level 3D representation  $\mathbf{z}$  from  $\mathcal{C}$ , such that target image  $\mathbf{x}_q$  from arbitrary query viewpoint  $\mathbf{v}_q$  can be generated by the decoder  $p(\mathbf{x}_q | \mathbf{z}, \mathbf{v}_q)$ . The generative process can be written:

$$p(\mathbf{x}_q | \mathbf{v}_q, \mathcal{C}) = \int p(\mathbf{x}_q | \mathbf{z}, \mathbf{v}_q) p(\mathbf{z} | \mathcal{C}) d\mathbf{z}. \quad (1)$$

The prior encoder  $p(\mathbf{z} | \mathcal{C})$  first obtains an order-invariant encoding  $\mathbf{r}_\mathcal{C}$  of context  $\mathcal{C}$ , and then uses ConvDRAW [18] to sample  $\mathbf{z}$  from  $\mathbf{r}_\mathcal{C}$ . Since the posterior distribution  $p(\mathbf{z} | \mathbf{x}_q, \mathbf{v}_q, \mathcal{C})$  is intractable, GQN performs variational inference for posterior approximation by maximizing its evidence lower bound. Backpropagation through random variables is done by the reparameterization trick [28].

Note that the model described above is actually a more consistent version of the GQN (CGQN) [31]. In the original GQN [13], the latent  $\mathbf{z}$  is also conditioned on  $\mathbf{v}_q$  and rendering is query-agnostic, i.e.,  $p(\mathbf{x}_q | \mathbf{z})$ , leading to some inconsistency across multiple query viewpoints. Throughout the paper, we use the abbreviation GQN to refer to the general GQN framework embracing both GQN and CGQN.

## 3 ROOTS

GQN represents a multi-object scene as a single vector without explicit object-wise decomposition. In this section, we propose ROOTS, a probabilistic generative model that learns to build individual models of 3D objects from scene images. Provided the context  $\mathcal{C}$ , ROOTS yields individual 3D object models. Each model can infer a 3D representation and render the object. The learned object model is modular and compositional so that we can also reconstruct the full scene from arbitrary viewpoints by compositing the individual 3D object models. ROOTS consists of five stages. From the context, the ROOTS encoder obtains 3D representations for individual objects through three stages (i) Scene Encoding, (ii) Object-Attention Grouping, and (iii) Object Encoding. Then, the ROOTS decoder renders each object according to a query viewpoint and composites the full scene via (iv) Object Renderer and (v) Scene Composer. The entire process is unsupervised and end-to-end trained. See Figure 1 for an illustrative overview of this process.

### 3.1 ROOTS Encoder

**Scene Encoder.** The goal of the scene encoder is to infer the positions of each object in the 3D scene by mapping the 3D space into a canonical 3D map. To efficiently deal with the variable number of objects, the model partitions the 3D map into  $N_{\max} = N_x \times N_y \times N_z$  cells, each responsible for detecting at most one object. Specifically, let  $(i, j, k)$  be the index of a cell. For each cell, we introduce a Bernoulli variable  $z_{ijk}^{\text{pres}} \in \{0, 1\}$  to denote whether there is an object whose center position (not the whole volume of the object) is within the cell, and if so, we infer a continuous latent  $\mathbf{z}_{ijk}^{\text{where}} \in \mathbb{R}^3$  to specify the center position of that object in the canonical coordinate system.

To detect objects that are close to each other, one option is to increase the number of cells, which is a hyperparameter controlling the object density. However, this also increases the computational cost. Hence, we instead let the neighboring cells have some overlap in 3D space, so that the scene encoder can learn to distribute nearby objects to adjacent cells rather than detect only one of them.

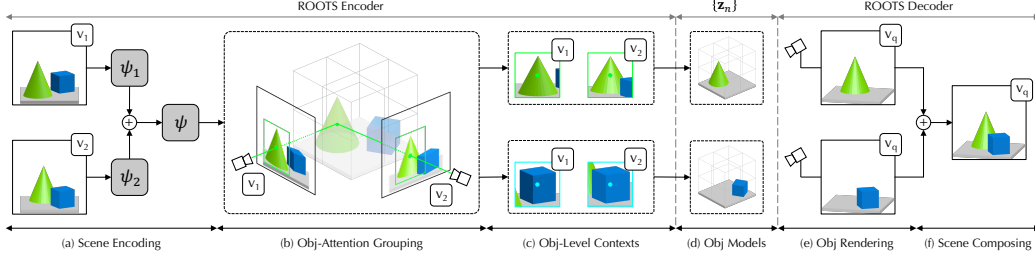


Figure 1: Overview of ROOTS pipeline.

To infer  $\{(z_{ijk}^{\text{pres}}, z_{ijk}^{\text{where}})\}$  from the collection of context observations  $\mathcal{C} = \{(\mathbf{x}_c, \mathbf{v}_c)\}$ , we encode  $\mathcal{C}$  into a Geometric Volume Feature Map (GVFM)  $\mathbf{r} \in \mathbb{R}^{N_x \times N_y \times N_z \times d}$ , yielding a  $d$ -dimensional feature vector  $\mathbf{r}_{ijk}$  for each cell. Then,  $\{(z_{ijk}^{\text{pres}}, z_{ijk}^{\text{where}})\}$  can be computed in parallel for all cells:

$$p(z_{ijk}^{\text{pres}}, z_{ijk}^{\text{where}} | \mathcal{C}) = f_{\text{pres, where}}(\mathbf{r}_{ijk}^{\text{neighbor}}), \quad (2)$$

where  $\mathbf{r}_{ijk}^{\text{neighbor}}$  denotes the feature vectors of cell  $(i, j, k)$  and its neighboring cells, allowing inter-object relations to be taken into consideration.

We note that GVFM shares some similarities with the grid cells used in SPAIR [9] and SPACE [34]. However, as a feature map of the 3D space, GVFM must *aggregate* information from multiple partial 2D observations and *reorganize* it in an object-wise fashion. This is in contrast to the 2D feature map learned by grid cells which have a natural alignment with the single fully-observed 2D image. Therefore, we obtain GVFM in two steps. First, we compute an order-invariant summary  $\psi$  of  $\mathcal{C}$  as the summation over encodings of individual context observations:  $\psi = \sum_{c=1}^{|\mathcal{C}|} \psi_c = \sum_{c=1}^{|\mathcal{C}|} f_{\psi}(\mathbf{x}_c, \mathbf{v}_c)$ . Second, we apply a 3D transposed convolution over  $\psi$  to split the scene-level representation  $\psi$  into individual  $\mathbf{r}_{ijk}$  slots containing object-specific information.

**Object-Attention Grouping.** One crucial operation in obtaining object-wise appearance representation, known as object-attention grouping, is to identify an image region that contains a single object [12, 9, 34]. The main challenge in our 3D setting is that such attention has to be *consistent* – finding image regions that correspond to the same object across different context observations. More precisely, for each object  $n$  present in the scene and each context image  $\mathbf{x}_c$ , we seek a 2D bounding box capturing object  $n$  in  $\mathbf{x}_c$ . The bounding box is parameterized by its center position and scale (width and height), denoted by  $(\mathbf{o}_{n,c}^{\text{center}}, \mathbf{o}_{n,c}^{\text{scale}})$ .

We propose to achieve consistent object-attention grouping by perspective projection [19]. Our key insight is that by projecting the 3D center position  $\mathbf{z}_n^{\text{where}}$  of an object onto the image plane, we can find its precise 2D location in each context image. This is more efficient than the Epipolar Cross-Attention [46] which attends to an epipolar line rather than a single position.

**Attention-by-Perspective-Projection (APP).** Let  $\mathbf{z}_n^{\text{where}}$  be the 3D center position of object  $n$ .  $\text{APP}_{\text{pos}}$  computes  $\mathbf{o}_{n,c}^{\text{center}}$  along with  $\mathbf{o}_{n,c}^{\text{depth}}$ , the distance between object  $n$  and the camera as follows:

$$[\mathbf{o}_{n,c}^{\text{center}}, \mathbf{o}_{n,c}^{\text{depth}}]^\top = \text{APP}_{\text{pos}}(\mathbf{z}_n^{\text{where}}, \mathbf{v}_c) = \text{normalize}(\mathbf{T}_{\text{World-Camera}}(\mathbf{v}_c)[\mathbf{z}_n^{\text{where}}, 1]^\top). \quad (3)$$

Here,  $\mathbf{z}_n^{\text{where}}$  is first converted to the camera coordinates by the viewpoint-dependent transformation matrix  $\mathbf{T}_{\text{World-Camera}}(\mathbf{v}_c) \in \mathbb{R}^{3 \times 4}$ , and then normalized. See the supplementary material for more details.

To compute  $\mathbf{o}_{n,c}^{\text{scale}}$ , one option is to learn a 3D bounding box for object  $n$ , and then project its eight vertices onto the image plane. Unfortunately, this hardwired projection often yields inaccurate results. Hence, we design  $\text{APP}_{\text{scale}}$  to also learn the projection:

$$\mathbf{o}_{n,c}^{\text{scale}} = \text{APP}_{\text{scale}}(\mathbf{o}_{n,c}^{\text{center}}, \mathbf{o}_{n,c}^{\text{depth}}, \mathbf{r}_n, \mathbf{v}_c) = \text{MLP}(\text{concat}[\mathbf{o}_{n,c}^{\text{center}}, \mathbf{o}_{n,c}^{\text{depth}}, \mathbf{r}_n, \mathbf{v}_c]). \quad (4)$$

$\text{APP}_{\text{scale}}$  implicitly builds the 3D bounding box from  $\mathbf{r}_n$ , projects it onto the image plane from viewpoint  $\mathbf{v}_c$ , and refines the projected bounding box using  $\mathbf{o}_{n,c}^{\text{center}}$  and  $\mathbf{o}_{n,c}^{\text{depth}}$ .

**Object Encoder.** With consistent object-attention grouping, we can decompose the scene-level context  $\mathcal{C}$  into object-level context  $\mathcal{C}_n$  for each object  $n = 1, \dots, N$ , where  $N = \sum_{ijk} z_{ijk}^{\text{pres}} \leq N_{\text{max}}$  is the total number of objects present in the scene. Specifically, we first use a spatial transformer

$\mathcal{ST}$  [22] to crop local image patches  $\mathbf{x}_{n,c}^{\text{att}}$  from observation  $\mathbf{x}_c$  using  $\mathbf{o}_{n,c}^{\text{center}}$  and  $\mathbf{o}_{n,c}^{\text{scale}}$ . After collecting these patches from all viewpoints, we group them based on the object index  $n$  to obtain  $\mathcal{C}_n = \{(\mathbf{x}_{n,c}^{\text{att}}, \mathbf{v}_c, \mathbf{o}_{n,c}^{\text{where}})\}_{c=1}^C$ , where we include  $\mathbf{o}_{n,c}^{\text{where}} = (\mathbf{o}_{n,c}^{\text{center}}, \mathbf{o}_{n,c}^{\text{scale}}, \mathbf{o}_{n,c}^{\text{depth}})$  to provide information complementary to  $\mathbf{x}_{n,c}^{\text{att}}$ . This process of obtaining  $\{\mathcal{C}_n\}_{n=1}^N$  allows us to utilize an object-level GQN encoder  $p(\mathbf{z}_n^{\text{what}} | \mathcal{C}_n) = \text{GQN}_{\text{enc}}(\mathcal{C}_n)$  to obtain independent and modular object-level 3D representation  $\mathbf{z}_n^{\text{what}}$  for each object  $n$ .

### 3.2 ROOTS Decoder

Given partial observations of a multi-object 3D scene, ROOTS not only learns the 3D representation of individual objects, but also learns to render them independently and individually. The full scene can be rendered from arbitrary query viewpoints by the composition of the object renderings. Thus, ROOTS can easily generate novel scenes that are out of the training distribution.

**Object Renderer.** For each object  $n$ , given its 3D representation  $\mathbf{z}_n^{\text{what}}$  and a query viewpoint  $\mathbf{v}_q$ , ROOTS is able to generate an image  $\mathbf{o}_{n,q}^{\text{what}}$  depicting the object’s appearance when viewed from  $\mathbf{v}_q$ . This is achieved through an object-level GQN decoder:  $\mathbf{o}_{n,q}^{\text{what}} = \text{GQN}_{\text{dec}}(\mathbf{z}_n^{\text{what}}, \mathbf{r}_n^{\text{att}}, \mathbf{v}_q)$ , where  $\mathbf{r}_n^{\text{att}}$  is an order-invariant summary of object-level context  $\mathcal{C}_n$ .

**Scene Composer.** To composite the objects into a scene, they need to be placed at the right location with proper scaling. Our model allows us to simply reuse the APP module here and compute:

$$[\mathbf{o}_{n,q}^{\text{center}}, \mathbf{o}_{n,q}^{\text{depth}}]^\top = \text{APP}_{\text{pos}}(\mathbf{z}_n^{\text{where}}, \mathbf{v}_q), \text{ and } \mathbf{o}_{n,q}^{\text{scale}} = \text{APP}_{\text{scale}}(\mathbf{o}_{n,q}^{\text{center}}, \mathbf{o}_{n,q}^{\text{depth}}, \mathbf{r}_n, \mathbf{v}_q). \quad (5)$$

We then render a partial scene  $\hat{\mathbf{x}}_{n,q}$ , containing only object  $n$ , through an inverse spatial transformer:  $\hat{\mathbf{x}}_{n,q} = \mathcal{ST}^{-1}(\mathbf{o}_{n,q}^{\text{what}}, \mathbf{o}_{n,q}^{\text{center}}, \mathbf{o}_{n,q}^{\text{scale}})$ . This can be seen as an object-specific image layer. The last step is to composite these  $N$  layers into a single image so that occlusion among objects can be properly handled. Similar to previous works [9, 4, 16, 11, 51, 34], for each layer  $n$ , we compute a transparency map  $\alpha_{n,q}$  from  $\mathbf{o}_{n,q}^{\text{what}}$  and  $\mathbf{o}_{n,q}^{\text{depth}}$ , ensuring that objects with larger depth are occluded by objects with smaller depth. The final rendered scene  $\hat{\mathbf{x}}_q$  is composited as:  $\hat{\mathbf{x}}_q = \sum_{n=1}^N \alpha_{n,q} \odot \hat{\mathbf{x}}_{n,q}$ , where  $\odot$  is pixel-wise multiplication.

### 3.3 Inference and Learning

For simplicity, here we consider a single query viewpoint. The extension to multiple query viewpoints is straightforward. Let  $\mathcal{D} = \mathcal{C} \cup (\mathbf{x}_q, \mathbf{v}_q)$ . Due to the intractability of the true posterior, we train ROOTS using variational inference with the following posterior approximation:  $p(N, \{\mathbf{z}_n\}_{n=1}^N | \mathcal{D}) \approx q(N | \mathcal{D}) \prod_{n=1}^N q(\mathbf{z}_n^{\text{where}} | \mathcal{D}) q(\mathbf{z}_n^{\text{what}} | \mathcal{D}_n)$ , where  $\mathcal{D}_n$  is the object-level context obtained from  $\mathcal{D}$ . The implementation of approximate posterior is similar to ROOTS encoder as described in Section 3.1. The main difference is that the summary vector  $\psi$  should now encode the entire  $\mathcal{D}$ . The training objective is to maximize the following Evidence Lower Bound:

$$\mathcal{L} = \mathbb{E}_q[\log p(\mathbf{x}_q | \{\mathbf{o}_{n,q}\}) - D_{\text{KL}}[q(N | \mathcal{D}) \| p(N | \mathcal{C})] - \sum_{n=1}^N D_{\text{KL}}[q(\mathbf{z}_n | \mathcal{D}) \| p(\mathbf{z}_n | \mathcal{C})]]. \quad (6)$$

**Combining with Unconditioned Prior.** One difficulty in using the conditional prior is that it may not coincide with our prior knowledge of the latent variables. In our experiments, it turns out that biasing the posterior of some variables toward our prior preference helps stabilize the model. We achieve this by introducing some additional KL terms between the posterior and *unconditioned* prior (like in VAEs) to the ELBO. See the supplementary material for more details.

## 4 Related Work

**Geometric Deep Learning.** The computer vision community has studied the visual 3D learning from different perspectives from ours in the sense that they are either (i) not decomposing a scene of multiple objects into object-wise representations by mostly working on single-object scenes [52, 53, 6, 25, 36], (ii) using supervised approaches [20, 48, 5, 43, 10], (iii) learning image generation (synthesis) of a 3D scene without scene-representation [26, 39, 49] or without learning to render [55, 54], or (iv) not end-to-end trainable.

**Neural Representation of 3D Scenes.** Recent works [13, 31, 46, 44, 45, 35] have explored learning 3D scene representations from 2D images without 3D supervision. While the rendering quality has

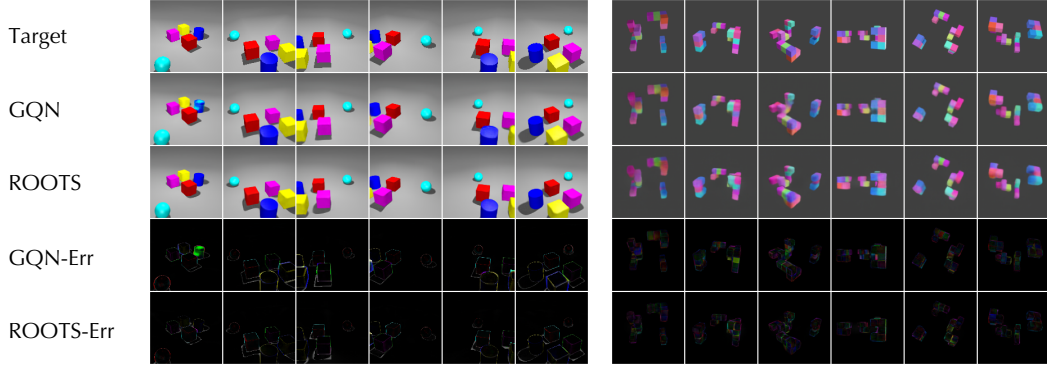


**Figure 2:** Sample generations from two scenes. Columns correspond to query viewpoints. ROOTS gives better generations in regions of occlusion while GQN sometimes misses occluded objects and predicts wrong colors.

been improved in [46, 45, 35], they are not able to decompose the full scene into objects and learn object-wise representation and rendering models. We believe these works are complementary to ROOTS and may allow object models to be learned from more realistic scenes. Another line of work [37, 33] learns object-aware 3D scene representations for generative adversarial networks [15]. They only support rendering and are unable to infer the object models for a given scene.

**Object-Oriented Representation of 2D Images.** There have been prolific advances in unsupervised object-oriented representation learning from fully-observed 2D images. They mainly fall into two categories: detection-based and mixture-based. The detection-based approaches [12, 9, 34] first identify object regions and then learn object representations from object patches cropped by the spatial transformer [22]. The mixture-based approaches [17, 4, 16, 11] model the observed image as a pixel-level Gaussian mixture where each component is expected to capture a single object. None of these approaches consider the 3D structure of the scene, let alone the 3D appearance of objects.

## 5 Experiments

**Datasets.** Our main focus is to evaluate the quality of learned object models and the benefits they bring in terms of generation quality, generalization ability, and downstream task performance. Existing datasets in [13, 46] either do not contain multi-object scenes or cannot provide object-wise groundtruth information like object positions, and thus cannot serve our purpose. Hence, we created two datasets: the Shapes dataset and the Multi-Shepard-Metzler (MSM) dataset, using MuJoCo [47] and Blender [7] respectively. Both datasets contain 60K multi-object scenes (50K for training, 5K for validation, and 5K for testing) with complete groundtruth scene specifications. Each scene is rendered as  $128 \times 128$  color images from 30 random viewpoints. Notice that the scene specifications are for evaluation only and are not used during training.

We generated three versions of the Shapes dataset, containing scenes with 1-3, 2-4, and 3-5 objects respectively. The position, size, shape, and color of the objects are randomized. The MSM dataset contains scenes with 2-4 randomly positioned Shepard-Metzler objects. Each object consists of 5 randomly colored cubes and is generated in the same way as described in [13]. Since these objects have complex shapes randomly generated per scene, they span a large combinatorial space and it is unlikely for an object to appear in multiple scenes. Also, the objects can have severe occlusion with each other, making this dataset significantly more challenging than the single-object version in [13].

**Baseline.** Because there is no previous work that can build 3D object models from multi-object scene images, we use separate baselines to evaluate scene-level representation and object-level decomposition respectively. For scene-level representation and generation quality, we use CGQN [31] as the baseline model, and refer to it as GQN in the rest of this section to indicate the general GQN framework. For object-level decomposition, we compare the image segmentation ability embedded in ROOTS with that of IODINE [16], which focuses on this ability without learning 3D representations.

### 5.1 Qualitative Evaluation

**Scene Generation.** Like GQN, ROOTS is able to generate target observations for a given scene from arbitrary query viewpoints. Figure 2 shows a comparison of scene generations using 15 contexts.

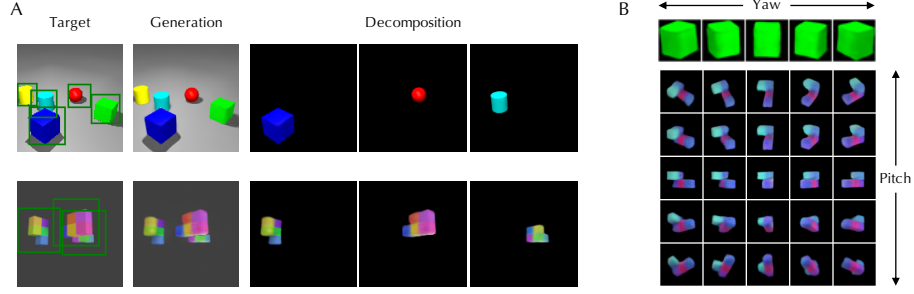


**Figure 3:** (A) The full scene is composited from individual object rendering results (not all objects are shown). Predicted bounding boxes are drawn on target images. (B) Visualization of learned object models from a set of query viewpoints. ROOTS learns the complete 3D object appearance, predicts accurate object positions, and correctly handles occlusion.

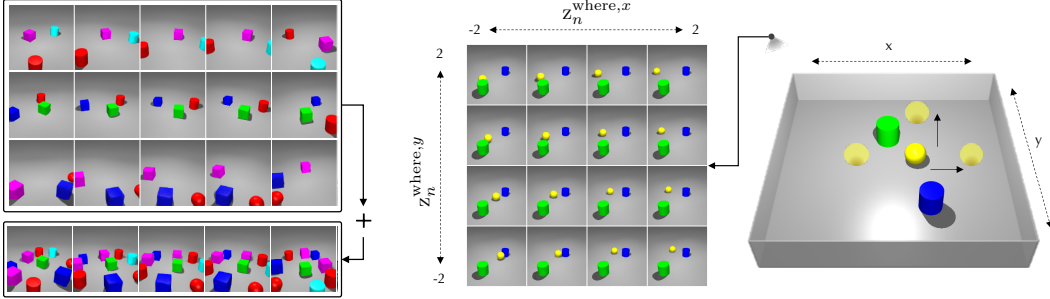


**Figure 4:** Learned object models are re-configured into a novel scene. Columns correspond to query viewpoints.

**Figure 5:** Traversal of the position latent  $z_n^{\text{where},x}$  and  $z_n^{\text{where},y}$  of the yellow ball in the scene (right). We show generations (left) from a query viewpoint after manipulating the position latent.

ROOTS gives better generations in regions of occlusion while GQN sometimes misses occluded objects and predicts wrong colors. We also found for both datasets that GQN often generated color inconsistency within an object as shown in Figure 2. ROOTS, having object-level modular rendering, was more robust to this problem. For the Multi-Shepard-Metzlerdataset, GQN samples might look slightly clearer than those of ROOTS as it generates clearer boundaries between the unit cubes compositing a block. However, the difference map reveals that GQN more frequently draws the objects with wrong colors.

**Object Models.** We believe that the object models learned by ROOTS provide a stronger capacity to represent the appearance of individual objects, leading to its better generation quality mentioned above. We further visualize the learned object models in Figure 3B, by applying the object renderer to  $z_n^{\text{what}}$  and a set of query viewpoints. We also show the scene rendering process in Figure 3A, where object rendering results are composited to generate the full scene. As can be seen, from images containing multiple objects with occlusion, ROOTS is able to learn the complete 3D appearance model of each object, predict accurate object positions, and correctly handle occlusion. Such object models are not available from GQN because it only learns scene-level representation.

**Compositionality.** Once object models are learned, they can be reconfigured to form novel scenes that are out of the training distribution. As an example, in Figure 4, we first provide ROOTS with context images from three scenes (top three rows) with 3 objects each, and collect the learned object representations  $\{(r_n^{\text{att}}, z_n^{\text{where}}, z_n^{\text{what}})\}$ . A new scene with 9 objects can then be composed and rendered from arbitrary query viewpoints. Rendering results are shown in the bottom row of Figure 4. We would like to emphasize that the model is trained on scenes with 1-3 objects. Thus, a scene with 9 objects has never been seen during training.

**Disentanglement.** Since object position and appearance are disentangled in the learned object models, by manipulating the position latent, we are able to move objects around without changing other factors like object appearance. In Figure 5, we visualize traversals of  $z_n^{\text{where},x}$  and  $z_n^{\text{where},y}$  of the yellow ball through generations from a query viewpoint. It can be seen that the change of one coordinate does not affect the other. In addition, the appearance of the yellow ball remains complete and clean during the traversal. Other untouched components (the green cylinder, the blue cylinder,

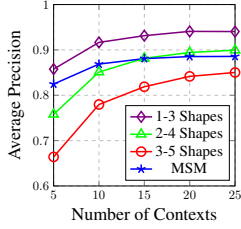


**Figure 6:** Average precision and counting accuracy.

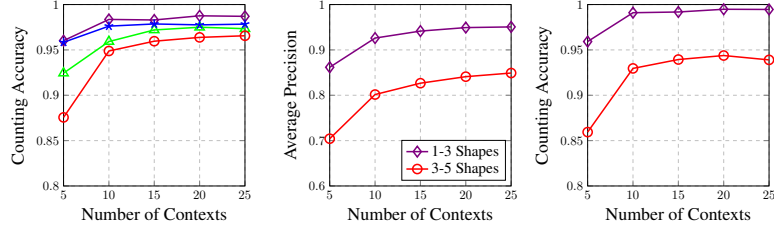


**Figure 7:** Generalization performance of average precision and counting accuracy.

and background) remain unchanged. Moreover, we also notice some desired rendering effects. For example, the size of the yellow ball becomes smaller as it moves further away from the camera.

## 5.2 Quantitative Evaluation

**Scene Generation.** To compare the generation quality of ROOTS and GQN, in Table 1, we report negative log-likelihood (NLL) and mean squared error (MSE) on the test sets. We provide 15 context observations for both models, and use 100 samples to approximate NLL. Similar to previous works [31, 2], we report the minimum MSE over 100 samples from the learned conditional prior. This measures the ability of a conditional generative model to capture the true outcome within its conditional prior of all possible outcomes. ROOTS outperforms GQN on both metrics, showing that learning object models also contributes to better generation quality.

**Object Models.** To evaluate the quality of learned object models, we report object counting accuracy and an adapted version of Average Precision (AP) [14] in Figure 6. AP measures the object localization ability. To compute AP, we set some thresholds  $t_i$  on the 3D distance between the predicted  $\mathbf{z}_n^{\text{where}}$  and the groundtruth object center position. If the distance is within the threshold, the prediction is considered a true positive. Clearly, a smaller threshold requires the model to locate objects more accurately. We set three thresholds:  $1/4$ ,  $2/4$ , and  $3/4$  of the average object size. For each threshold  $t_i$ , we obtain the area under the precision-recall curve as  $\text{AP}(t_i)$ . The final AP is averaged over the three thresholds:  $\text{AP} = \sum_{i=1}^3 \text{AP}(t_i)/3$ . We vary the number of contexts provided, and compute counting accuracy and AP using the predicted  $N$  and  $\mathbf{z}_n^{\text{where}}$  that achieve the minimum MSE over 10 samples from the conditional prior. As shown in Figure 6, both counting accuracy and AP increase as the number of context observations becomes larger. This indicates that ROOTS can effectively accumulate information from the given contexts.

**Segmentation of 2D Observations.** The rendering process of ROOTS implicitly segments 2D observations under query viewpoints. The segmentation performance reflects the quality of learned 3D object appearance. Since GQN cannot provide such segmentation, we compare ROOTS with IODINE [16] in terms of the Adjusted Rand Index (ARI) [40, 21] on the Shapes datasets (IODINE failed on the MSM dataset). We train IODINE on all the images available in the training set, using the official implementation. At test time, ROOTS is given 15 random contexts for each scene and performs segmentation for an unseen query viewpoint. ROOTS does not have access to the target image under the query viewpoint. In contrast, IODINE directly takes the target image as input. Results in Table 2 show that ROOTS outperforms IODINE on both foreground segmentation (ARI-nobg) and full image segmentation (ARI).

**Generalization.** To evaluate the generalization ability, we first train ROOTS and GQN on the Shapes dataset with 2-4 objects, and then test on the Shapes datasets with 1-3 objects and 3-5 objects respectively. As shown in Table 3, ROOTS achieves better NLL and MSE in both interpolation and

**Table 1:** Negative log-likelihood (NLL) and minimum mean squared error (MSE).

Testing Set	1-3 Shapes		2-4 Shapes		3-5 Shapes		Multi-Shepard-Metzler	
Metrics	NLL	MSE	NLL	MSE	NLL	MSE	NLL	MSE
ROOTS	-207595.81	30.60	-206611.07	42.41	-205608.07	54.45	-206627.56	42.22
GQN	-206760.87	40.62	-205604.74	54.49	-204918.39	62.73	-206294.22	46.22



**Table 2:** Quantitative evaluation of 2D segmentation.

Testing Set	1-3 Shapes		2-4 Shapes		3-5 Shapes		Multi-Shepard-Metzler	
Metrics	ARI	ARI-nobg	ARI	ARI-nobg	ARI	ARI-nobg	ARI	ARI-nobg
ROOTS	0.9477	0.9942	0.9482	0.9947	0.9490	0.9930	0.9303	0.9608
IODINE	0.8217	0.8685	0.8348	0.9854	0.8422	0.9580	N/A	N/A

**Table 3:** Quantitative evaluation of generalization ability.

Testing Set	1-3 Shapes		3-5 Shapes	
Metrics	NLL	MSE	NLL	MSE
ROOTS	-208122.58	24.27	-204480.37	67.98
GQN	-207616.49	30.35	-202922.03	86.68

**Table 4:** Testing accuracies on downstream tasks.

Tasks	Retrieve Object		Find Pair
	3D Version	2D Version	
ROOTS	90.38%	93.71%	84.70%
GQN	81.31%	84.18%	12.48%

extrapolation settings. We further report AP and counting accuracy for ROOTS when generalizing to the above two datasets. As shown in Figure 7, ROOTS generalizes well to scenes with 1-3 objects, and performs reasonably when given more context observations on scenes with 3-5 objects.

**Downstream 3D Reasoning Tasks.** The 3D object models can facilitate object-wise 3D reasoning. We demonstrate this in two downstream tasks on the Shapes dataset with 3-5 objects. **Retrieve Object.** The goal of this task is to retrieve the object that lies closest to a given position  $p$ . We consider both 3D and 2D versions of the task. In 3D version, we set  $p$  as the origin of the 3D space, whereas in 2D version,  $p$  is the center point of the target image from viewpoint  $v_q$ . We treat this task as a classification problem, where the input is the learned representation (along with  $v_q$  in 2D version), and the output is the label of the desired object. Here, the label is an integer assigned to each object based on its shape and color. We compare ROOTS with the GQN baseline, and report testing accuracies in Table 4. ROOTS outperforms GQN, demonstrating the effectiveness of the learned object models in spatial reasoning. **Find Pair.** In this task, the goal is to find two objects that have the smallest pair-wise distance in 3D space. Again, we treat this as a classification task, where the target label is the sum of labels of the two desired objects. The testing accuracies are reported in Table 4. Clearly, this task requires pair-wise relational reasoning. The object models learned by ROOTS naturally allows extraction of pair-wise relations. In contrast, the scene-level representation of GQN without object-wise factorization leads to incompetence in relational reasoning.

### 5.3 Ablation Study

Our ablation study shows that the components of ROOTS are necessary for obtaining object models. In particular, we tried the following alternative design choices. **ROOTS Encoder.** One may think that  $\mathbf{z}_n^{\text{what}}$  can be directly inferred from scene-level contexts without object-attention grouping. Thus, we tried inferring  $\mathbf{z}_n^{\text{what}}$  from GVFM along with  $\mathbf{z}_n^{\text{pres}}$  and  $\mathbf{z}_n^{\text{where}}$ . The model, however, failed to decompose scenes into objects and hence was not trainable. **ROOTS Decoder.** One may also think that the object-specific image layer  $\hat{\mathbf{x}}_{n,q}$  can be directly generated from the 3D representation  $\mathbf{z}_n$  without having intermediate 2D representation  $\mathbf{o}_{n,q}$ . This model was also not trainable as it could not use the object positions effectively.

## 6 Conclusion

We proposed ROOTS, a probabilistic generative model for unsupervised learning of 3D object models from partial observations of multi-object 3D scenes. The learned object models capture the complete 3D appearance of individual objects, yielding better generation quality of the full scene. They also improve generalization ability and allow out-of-distribution scenes to be easily generated. Moreover, in downstream 3D reasoning tasks, ROOTS shows superior performance compared to the baseline model. Interesting future directions would be to learn the knowledge of the 3D world in a sequential manner as we humans keep updating our knowledge of the world.



## Acknowledgement

SA thanks Kakao Brain and Center for Super Intelligence (CSI) for their support. The authors thank Jindong Jiang for helpful discussion.

## References

- [1] Martin Arjovsky, Léon Bottou, Ishaan Gulrajani, and David Lopez-Paz. Invariant risk minimization. *arXiv preprint arXiv:1907.02893*, 2019.
- [2] Mohammad Babaeizadeh, Chelsea Finn, Dumitru Erhan, Roy H Campbell, and Sergey Levine. Stochastic variational video prediction. *arXiv preprint arXiv:1710.11252*, 2017.
- [3] Léon Bottou. From machine learning to machine reasoning. *Machine learning*, 94(2):133–149, 2014.
- [4] Christopher P Burgess, Loic Matthey, Nicholas Watters, Rishabh Kabra, Irina Higgins, Matt Botvinick, and Alexander Lerchner. Monet: Unsupervised scene decomposition and representation. *arXiv preprint arXiv:1901.11390*, 2019.
- [5] Ricson Cheng, Ziyang Wang, and Katerina Fragkiadaki. Geometry-aware recurrent neural networks for active visual recognition. In *Advances in Neural Information Processing Systems*, pages 5081–5091, 2018.
- [6] Christopher B Choy, Danfei Xu, JunYoung Gwak, Kevin Chen, and Silvio Savarese. 3d-r2n2: A unified approach for single and multi-view 3d object reconstruction. In *European conference on computer vision*, pages 628–644. Springer, 2016.
- [7] Blender Online Community. *Blender - a 3D modelling and rendering package*. Blender Foundation, Stichting Blender Foundation, Amsterdam, 2018.
- [8] Eric Crawford and Joelle Pineau. Exploiting spatial invariance for scalable unsupervised object tracking. *arXiv preprint arXiv:1911.09033*, 2019.
- [9] Eric Crawford and Joelle Pineau. Spatially invariant unsupervised object detection with convolutional neural networks. In *Proceedings of the AAAI Conference on Artificial Intelligence*, volume 33, pages 3412–3420, 2019.
- [10] Yilun Du, Zhijian Liu, Hector Basevi, Ales Leonardis, Bill Freeman, Josh Tenenbaum, and Jiajun Wu. Learning to exploit stability for 3d scene parsing. In *Advances in Neural Information Processing Systems*, pages 1726–1736, 2018.
- [11] Martin Engelcke, Adam R. Kosior, Oivi Parker Jones, and Ingmar Posner. Genesis: Generative scene inference and sampling with object-centric latent representations. In *International Conference on Learning Representations*, 2020.
- [12] SM Ali Eslami, Nicolas Heess, Theophane Weber, Yuval Tassa, David Szepesvari, Geoffrey E Hinton, et al. Attend, infer, repeat: Fast scene understanding with generative models. In *Advances in Neural Information Processing Systems*, pages 3225–3233, 2016.
- [13] SM Ali Eslami, Danilo Jimenez Rezende, Frederic Besse, Fabio Viola, Ari S Morcos, Marta Garnelo, Avraham Ruderman, Andrei A Rusu, Ivo Danihelka, Karol Gregor, David P Reichert, Lars Buesing, Theophane Weber, Oriol Vinyals, Dan Rosenbaum, Neil Rabinowitz, Helen King, Chloe Hillier, Matt Botvinick, Daan Wierstra, Koray Kavukcuoglu, and Demis Hassabis. Neural scene representation and rendering. *Science*, 360(6394):1204–1210, 2018.
- [14] Mark Everingham, Luc Van Gool, Christopher KI Williams, John Winn, and Andrew Zisserman. The pascal visual object classes (voc) challenge. *International journal of computer vision*, 88(2):303–338, 2010.
- [15] Ian Goodfellow, Jean Pouget-Abadie, Mehdi Mirza, Bing Xu, David Warde-Farley, Sherjil Ozair, Aaron Courville, and Yoshua Bengio. Generative adversarial nets. In *Advances in neural information processing systems*, pages 2672–2680, 2014.
- [16] Klaus Greff, Raphaël Lopez Kaufman, Rishabh Kabra, Nick Watters, Christopher Burgess, Daniel Zoran, Loic Matthey, Matthew Botvinick, and Alexander Lerchner. Multi-object representation learning with iterative variational inference. In *International Conference on Machine Learning*, pages 2424–2433, 2019.

- [17] Klaus Greff, Sjoerd Van Steenkiste, and Jürgen Schmidhuber. Neural expectation maximization. In *Advances in Neural Information Processing Systems*, pages 6691–6701, 2017.
- [18] Karol Gregor, Frederic Besse, Danilo Jimenez Rezende, Ivo Danihelka, and Daan Wierstra. Towards conceptual compression. In *Advances In Neural Information Processing Systems*, pages 3549–3557, 2016.
- [19] Richard Hartley and Andrew Zisserman. *Multiple view geometry in computer vision*. Cambridge university press, 2003.
- [20] Siyuan Huang, Siyuan Qi, Yinxue Xiao, Yixin Zhu, Ying Nian Wu, and Song-Chun Zhu. Cooperative holistic scene understanding: Unifying 3d object, layout, and camera pose estimation. In *Advances in Neural Information Processing Systems*, pages 207–218, 2018.
- [21] Lawrence Hubert and Phipps Arabie. Comparing partitions. *Journal of classification*, 2(1):193–218, 1985.
- [22] Max Jaderberg, Karen Simonyan, Andrew Zisserman, and Koray Kavukcuoglu. Spatial transformer networks. In *Advances in neural information processing systems*, pages 2017–2025, 2015.
- [23] Jindong Jiang, Sepehr Janghorbani, Gerard De Melo, and Sungjin Ahn. Scalor: Generative world models with scalable object representations. In *International Conference on Learning Representations*, 2020.
- [24] Philip N Johnson-Laird. Mental models and human reasoning. *Proceedings of the National Academy of Sciences*, 107(43):18243–18250, 2010.
- [25] Abhishek Kar, Christian Häne, and Jitendra Malik. Learning a multi-view stereo machine. In *Advances in neural information processing systems*, pages 365–376, 2017.
- [26] Hiroharu Kato and Tatsuya Harada. Learning view priors for single-view 3d reconstruction. In *Proceedings of the IEEE Conference on Computer Vision and Pattern Recognition*, pages 9778–9787, 2019.
- [27] Georg B Keller and Thomas D Mrsic-Flogel. Predictive processing: a canonical cortical computation. *Neuron*, 100(2):424–435, 2018.
- [28] Diederik P Kingma and Max Welling. Auto-encoding variational bayes. *arXiv preprint arXiv:1312.6114*, 2013.
- [29] Adam Kosior, Hyunjik Kim, Yee Whye Teh, and Ingmar Posner. Sequential attend, infer, repeat: Generative modelling of moving objects. In *Advances in Neural Information Processing Systems*, pages 8606–8616, 2018.
- [30] Jannik Kossen, Karl Stelzner, Marcel Hussing, Claas Voelcker, and Kristian Kersting. Structured object-aware physics prediction for video modeling and planning. *arXiv preprint arXiv:1910.02425*, 2019.
- [31] Ananya Kumar, SM Eslami, Danilo J Rezende, Marta Garnelo, Fabio Viola, Edward Lockhart, and Murray Shanahan. Consistent generative query networks. *arXiv preprint arXiv:1807.02033*, 2018.
- [32] Brenden M Lake, Tomer D Ullman, Joshua B Tenenbaum, and Samuel J Gershman. Building machines that learn and think like people. *Behavioral and brain sciences*, 40, 2017.
- [33] Yiyi Liao, Katja Schwarz, Lars Mescheder, and Andreas Geiger. Towards unsupervised learning of generative models for 3d controllable image synthesis. *arXiv preprint arXiv:1912.05237*, 2019.
- [34] Zhixuan Lin, Yi-Fu Wu, Skand Vishwanath Peri, Weihao Sun, Gautam Singh, Fei Deng, Jindong Jiang, and Sungjin Ahn. Space: Unsupervised object-oriented scene representation via spatial attention and decomposition. In *International Conference on Learning Representations*, 2020.
- [35] Ben Mildenhall, Pratul P Srinivasan, Matthew Tancik, Jonathan T Barron, Ravi Ramamoorthi, and Ren Ng. Nerf: Representing scenes as neural radiance fields for view synthesis. *arXiv preprint arXiv:2003.08934*, 2020.
- [36] Thu Nguyen-Phuoc, Chuan Li, Lucas Theis, Christian Richardt, and Yong-Liang Yang. Hologan: Unsupervised learning of 3d representations from natural images. *arXiv preprint arXiv:1904.01326*, 2019.

- [37] Thu Nguyen-Phuoc, Christian Richardt, Long Mai, Yong-Liang Yang, and Niloy Mitra. Blockgan: Learning 3d object-aware scene representations from unlabelled images. *arXiv preprint arXiv:2002.08988*, 2020.
- [38] Jonas Peters, Dominik Janzing, and Bernhard Schölkopf. *Elements of causal inference: foundations and learning algorithms*. MIT press, 2017.
- [39] Pedro O Pinheiro, Negar Rostamzadeh, and Sungjin Ahn. Domain-adaptive single-view 3d reconstruction. In *Proceedings of the IEEE International Conference on Computer Vision*, pages 7638–7647, 2019.
- [40] W.M. Rand. Objective criteria for the evaluation of clustering methods. *Journal of the American Statistical Association*, 66(336):846–850, 1971.
- [41] Daniel L Schacter, Donna Rose Addis, Demis Hassabis, Victoria C Martin, R Nathan Spreng, and Karl K Szpunar. The future of memory: remembering, imagining, and the brain. *Neuron*, 76(4):677–694, 2012.
- [42] Bernhard Schölkopf. *Causality for machine learning*, 2019.
- [43] Daeyun Shin, Zhile Ren, Erik B Sudderth, and Charless C Fowlkes. 3d scene reconstruction with multi-layer depth and epipolar transformers. In *Proceedings of the IEEE International Conference on Computer Vision*, pages 2172–2182, 2019.
- [44] Vincent Sitzmann, Justus Thies, Felix Heide, Matthias Nießner, Gordon Wetzstein, and Michael Zollhofer. Deepvoxels: Learning persistent 3d feature embeddings. In *Proceedings of the IEEE Conference on Computer Vision and Pattern Recognition*, pages 2437–2446, 2019.
- [45] Vincent Sitzmann, Michael Zollhöfer, and Gordon Wetzstein. Scene representation networks: Continuous 3d-structure-aware neural scene representations. In *Advances in Neural Information Processing Systems*, pages 1119–1130, 2019.
- [46] Joshua Tobin, Wojciech Zaremba, and Pieter Abbeel. Geometry-aware neural rendering. In *Advances in Neural Information Processing Systems*, pages 11555–11565, 2019.
- [47] Emanuel Todorov, Tom Erez, and Yuval Tassa. Mujoco: A physics engine for model-based control. In *2012 IEEE/RSJ International Conference on Intelligent Robots and Systems*, pages 5026–5033. IEEE, 2012.
- [48] Shubham Tulsiani, Saurabh Gupta, David F Fouhey, Alexei A Efros, and Jitendra Malik. Factoring shape, pose, and layout from the 2d image of a 3d scene. In *Proceedings of the IEEE Conference on Computer Vision and Pattern Recognition*, pages 302–310, 2018.
- [49] Shubham Tulsiani, Tinghui Zhou, Alexei A Efros, and Jitendra Malik. Multi-view supervision for single-view reconstruction via differentiable ray consistency. In *Proceedings of the IEEE conference on computer vision and pattern recognition*, pages 2626–2634, 2017.
- [50] Sjoerd van Steenkiste, Michael Chang, Klaus Greff, and Jürgen Schmidhuber. Relational neural expectation maximization: Unsupervised discovery of objects and their interactions. In *International Conference on Learning Representations*, 2018.
- [51] Sjoerd van Steenkiste, Karol Kurach, and Sylvain Gelly. A case for object compositionality in deep generative models of images. *arXiv preprint arXiv:1810.10340*, 2018.
- [52] Jiajun Wu, Chengkai Zhang, Tianfan Xue, Bill Freeman, and Josh Tenenbaum. Learning a probabilistic latent space of object shapes via 3d generative-adversarial modeling. In *Advances in neural information processing systems*, pages 82–90, 2016.
- [53] Xinchun Yan, Jimei Yang, Ersin Yumer, Yijie Guo, and Honglak Lee. Perspective transformer nets: Learning single-view 3d object reconstruction without 3d supervision. In *Advances in Neural Information Processing Systems*, pages 1696–1704, 2016.
- [54] Chong Yu and Young Wang. 3d-scene-gan: Three-dimensional scene reconstruction with generative adversarial networks. In *ICLR (Workshop)*, 2018.
- [55] Tinghui Zhou, Matthew Brown, Noah Snavely, and David G Lowe. Unsupervised learning of depth and ego-motion from video. In *Proceedings of the IEEE Conference on Computer Vision and Pattern Recognition*, pages 1851–1858, 2017.